Analysis of fracture behaviour in active materials for lithium ion batteries

Analysis of fracture behaviour in active materials for lithium ion batteries

Analysis of fracture behaviour in active materials for lithium ion batteries

D Clerici[1], F Mocera[1] and F Pistorio[1]

[1] Department of Mechanical and Aerospace Engineering, Politecnico di Torino, Corso duca degli Abruzzi 24, 10129 Torino, Italy

E-mail: davide.clerici@polito.it

Abstract. Several strong points make lithium ion battery one of the most widespread energy storage system. Nevertheless, one of the biggest drawbacks is the progressive damage which affects active materials, and influences cycle life as well. The hosting process of lithium ions causes the rise of mechanical stress in active material, which ultimately leads to the propagation of micro-flaws already present in fresh material. Finally, the damage of active material and solid-electrolyte interphase growth caused by cracks propagation result in capacity drop. The distribution of Mode I stress intensity factor is calculated along the semi-elliptical crack front on the outer surface and in the core of a three-dimensional spherical active material particle. A 3D and 2D finite element method analysis is performed in ANSYS Mechanical APDL starting from the mechanical stress state in active material computed with the electrochemical-mechanical model presented in previous works. The model is built using collapsed singular elements along the crack front, the not-singular version of these elements is used to model the outlying region of the crack area. The dependence of stress intensity factor on geometry size is deepened to evaluate the most critical condition. Moreover, the influence of current rate on stress intensity factor is investigated, in order to identify a current threshold beyond stress intensity factor is greater than the toughness of active material, and cracks start to propagate.

1. Introduction

Lithium ion battery (LIB) is nowadays the most common energy storage system, it meets the needs of a widespread field of applications, from small electronics up to heavy duty vehicles [1,2], thanks to its good energy and power density, great capacity and safe. Nevertheless, its nominal performance decreases during cycle life [3] and eventually it needs to be replaced after a certain number of cycles.

The aforementioned degradation is mainly correlated to mechanical damage of the electrodes [4]: lithium storage in electrode materials causes the rise of mechanical stress in the electrode itself, and leads to crack propagation ultimately, as deepened in previous studies [5,6].

Crack growth in electrode micro-structure causes two main problems: electrode isolation and SEI growth. Electrode isolation occurs when a portion of active material is detached and it can not host lithium ions anymore. On the other hand, cracks propagation causes the creation of new fresh surfaces of active material, where solid electrolyte interphase (SEI) precipitation can occur. The isolation of some portion of active material causes capacity fade and impedance rise, on the other hand, SEI precipitation consumes lithium ions that are no longer available to be cycled, then capacity fade occurs.

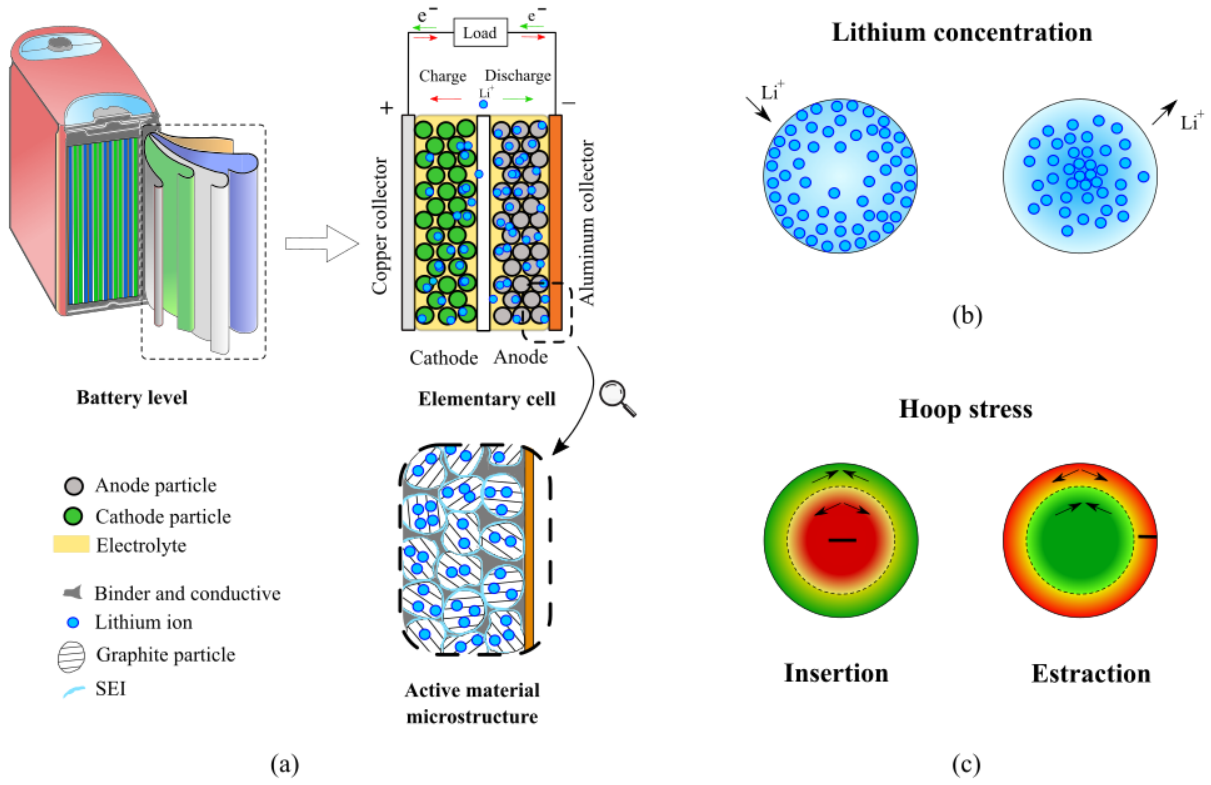

Figure 1: Battery model. (a) Internal structure of a typical LIB, from battery scale to micrometre scale. (b) Lithium concentration during intercalation and deintercalation: as lithium diffuses inside the particle, a concentration gradient is established, which leads to strain mismatch and stress. (c) Hoop stress distribution during intercalation and deintercalation. Hoop stress is compressive in the core and tensile on the surface during deintercalation, vice-versa during intercalation. Areas are marked with red where cracks can propagate and with green where cannot, as crack growth occurs just where hoop stress is tensile, according to mode I. As a consequence, internal cracks are likely to propagate during lithium insertion, and surface cracks during extraction.

A sketch of a typical LIB is reported in Figure 1a: battery is composed by several "elementary cells" that are made in turn by positive and negative current collectors, cathode, anode and separator. Each of the aforementioned components is a sheet few tens of micrometers thick. Cathode and anode are composed in turn by a mixture of several components, as shown in Figure 1a: Active material - a powder of quasi-spherical particles which occupies about 50% of the volume; Conductive materials and binder - about 20% in volume; finally 30% of volume is void, and is then occupied by liquid electrolyte. For this reason they are referred as porous electrodes.
Graphite is the most popular active material in negative electrode, whereas several metal oxides are used as positive electrode, such as: lithium iron phosphate (LFP), lithium cobalt oxide (LCO), lithium manganese oxide (LMO), Lithium nickel manganese cobalt oxide (NMC), Lithium nickel cobalt aluminium (NCA). These materials are known as intercalation materials, as lithium ions are intercalated into the interstices of the crystal structure. Lattice parameters vary according the lithium content, causing a volume increase during lithium intercalation, vice-versa during deintercalation. This behaviour may be seen in analogy with thermal strain: greater concentration (or temperature) gradient causes greater strain, following a linear trend,

where the proportionality coefficient is represented by fraction molar volume (or coefficient of thermal expansion).
Lithium ions diffuse inside the active material particles, causing an inhomogeneity in lithium concentration, as highlighted in Figure 1b, and thus a strain mismatch arises in the particle, leading to the so called diffusion induced stress (DIS) [5].
Mechanical stress caused by concentration gradient is the primary driving force of crack propagation [7–9]. Opening mode I, caused by a tensile stress normal to crack surfaces, is considered. Then, hoop stress is the driving force of crack propagation, as clarified in Figure 1c. Hoop stress is tensile on the surface during lithium deintercalation, and in the core during intercalation, as found in previous studies [5, 6]. This trend makes the cracks in the core to propagate during lithium intercalation, and those on the surface during deintercalation, as highlighted in Figure 1c.
Another effect which causes crack growth is phases transition [10, 11]. Some materials, such as LFP, present a strong boundary between li-rich and li-poor rather than a smooth gradient. The existence of two phases with a marked difference in lithium content causes a strong mechanical stress at the interface, which causes crack growth as well.
Fracture in active materials is affected by several factor: such as size and shape of the particle, size of pre-existing cracks and current rate [12]. Size and shape of the particle influences mechanical stress [13], indeed it was observed that small particles are less subjected to fracture because of smaller stress [12]. Current rate has a negative influence on cracks, as greater current rate causes greater stress, as well as longer pre-existing cracks makes their growth easier.
Crack modeling in LIB electrodes is still under debate in literature [12], several approaches are followed, such as phase field [14], cohesive model [15], energetic approaches [16]. In this work, a finite elements (FE) analysis in ANSYS Mechanical APDL is carried out on a spherical active material particle with superficial and internal cracks. Stress intensity factor is computed for different boundary conditions - namely current rates - to identify the boundary beyond unstable crack growth occurs. Several geometric configurations are considered to clarify their influence on crack propagation.

2. Fundamentals

2.1. Electrochemical-mechanical model

Fundamentals of electrochemical-mechanical modeling of active materials for LIB was treated in details in previous works [5, 6, 13], however a brief explanation is reported here as well.
Mechanical stress arises in the micro-structure of active material as a consequence of lithium inhomogeneity, caused by its diffusion through active material particle. As a consequence, this analysis involves two different fields: mechanical and electrochemical.
Mechanical model is expressed by Equations (1)-(3) according to the axisymmetric approach, where radial and circumferential are the directions needed to describe the problem. Constitutive Equations (1) show that a chemical strain $\frac{\Omega C}{3}$ is added to elastic strain, in analogy with what is usually done with thermal strain αT. It is straightforward to understand that an inhomogeneous concentration field can produce mechanical stress, exactly as temperature field does. At this stage, concentration field is needed to be solved in order to calculate mechanical stress.
Diffusion Equations (4)-(6) solve the concentration fields considering chemical potential, lithium flux and mass conservation equations. Flux of lithium ions goes from areas with high potential (high concentration) to areas with low potential (low concentration). This unbalanced concentration, and thus potential, is due to boundary flux, which is directly proportional to the current rate of the battery. Negative flux makes the lithium ions enter inside the particle, and diffuse towards the core, where concentration is lower. On the contrary, positive flux retrieves lithium ions from the surface and makes the ones in the core to diffuse towards the outer areas, where concentration is lowering.

Once concentration field is solved with a proper boundary flux, which can be expressed as current density I as well (Equation (7)), mechanical field is solved in turn (Equation (8)-(10)) considering radial stress to vanish on the external surface (free expansion), and constraining the central point of the particle in order to prevent rigid body motion. More complex surface constraints and contact characteristics between particles were deepened in a previous study [13].

Table 1: DIS model equations [5].

Mechanical equations		
Constitutive	$\sigma_r = \frac{E\left[\left(\varepsilon_r - \frac{\Omega c}{3}\right)(1-\nu) + 2\nu\left(\varepsilon_c - \frac{\Omega c}{3}\right)\right]}{(1+\nu)(1-2\nu)} \quad \sigma_c = \frac{E\left[\left(\varepsilon_c - \frac{\Omega c}{3}\right) + \nu\left(\varepsilon_r - \frac{\Omega c}{3}\right)\right]}{(1+\nu)(1-2\nu)}$	(1)
Congruence	$\varepsilon_r = \frac{du}{dr} \qquad \varepsilon_c = \frac{u}{r}$	(2)
Equilibrium	$\frac{d\sigma_r}{dr} + \frac{2}{r}\left(\sigma_r - \sigma_c\right) = 0$	(3)
Diffusion equations		
Chemical potential	$\mu = \mu_0 + R_g T ln(c)$	(4)
Flux	$J = -Mc\nabla\mu = -D\nabla c$	(5)
Mass conservation	$\frac{\partial c}{\partial t} + \nabla \cdot (\nabla J) = 0$	(6)
Solutions		
Concentration	$c(r,t) = c_0 + \frac{IR}{F_a D}\left[3\tau + \frac{1}{2}\left(\frac{r}{R}\right)^2 - \frac{3}{10} - 2\frac{R}{r}\sum_{n=1}^{\infty}\left(\frac{sin(\lambda_n r/R)}{\lambda_n^2 sin(\lambda_n)} e^{-\lambda_n^2 \tau}\right)\right]$	(7)
Displacement	$u(r) = \frac{\Omega}{3(1-\nu)}\left[(1+\nu)\frac{1}{r^2}\int_0^r c(r) r^2\, dr + 2(1-2\nu)\frac{r}{R^3}\int_0^R c(r) r^2\, dr\right]$	(8)
Radial stress	$\sigma_r(r) = \frac{2\Omega}{3}\frac{E}{1-\nu}\left[\frac{1}{R^3}\int_0^R c(r) r^2\ dr - \frac{1}{r^3}\int_0^r c(r) r^2\, dr\right]$	(9)
Hoop stress	$\sigma_c(r) = \frac{\Omega}{3}\frac{E}{1-\nu}\left[\frac{2}{R^3}\int_0^R c(r) r^2\ dr + \frac{1}{r^3}\int_0^r c(r) r^2\, dr - c(r)\right]$	(10)

2.2. Linear elastic fracture mechanics

Linear elastic fracture mechanics (LEFM) theory predicts the stress field singularity ahead the crack in terms of stress intensity factor and energy release rate G. This assumption holds whether the material is linear elastic or characterized by a small-scale yielding at the crack tip, i.e. the plastic zone extension at the crack tip is small relative to the crack length. The stress intensity factor K_I for a crack of characteristic size a and subjected to uniform tension σ in pure mode I

loading is:

$$K_I = Y\sigma\sqrt{\pi a} \tag{11}$$

where Y is the dimensionless geometric factor. The stress field describing the singularity near the crack tip in mode I loading can be expressed as follows:

$$\sigma_{ij} = \frac{K_I}{r_c^{1/2}} f_{ij}(\theta) \tag{12}$$

where σ_{ij} are the elastic stress components, r_c and θ are polar coordinates with origin at the crack tip, and $f_{ij}(\theta)$ is a dimensionless shape function. For a single fracture mode, the energy release rate G is a function of the stress intensity factor K_I:

$$G = \begin{cases} \dfrac{1}{E} K_I^2 & \text{plane stress} \\ \dfrac{1-\nu^2}{E} K_I^2 & \text{plane strain} \end{cases} \tag{13}$$

where E is the Young's modulus and ν is the Poisson's ratio. According to LEFM theory, the J-integral is a convenient way to calculate the energy release rate G. The 2D path-independent J-integral on an arbitrary counterclockwise path around the crack tip Γ, introduced by Rice [17], is defined as follows:

$$J = \int_\Gamma \left(W dx_2 - \mathbf{T} \frac{\partial \mathbf{u}}{\partial x_1} \right) ds \tag{14}$$

where W is the strain energy density, $\mathbf{T}$ is the traction vector on the path Γ of the outward unit normal vector $\mathbf{n}$, $\mathbf{u}$ is the displacement vector, x_1 and x_2 are the coordinate directions taken parallel and perpendicular to the crack direction, respectively. Using the divergence theorem, the J-integral can also be generalized to 3D by considering a tubular surface around the crack front. This domain integral method is used to evaluate contour integrals automatically in the FE analysis. The stress intensity factor K_I can be therefore computed from the J-integral by equating Equations (14) and (13).

According to LEFM, the onset of crack growth depends on the relative values of stress intensity factor and material-specific fracture toughness. The crack will propagate when the stress intensity factor exceeds the material fracture toughness. In the case of pure mode-I crack opening fracture occurs when:

$$K_I \geq K_{Ic} \tag{15}$$

where K_{Ic} is the fracture toughness relative to mode I loading.

3. Method

Fracture behaviour of active material particles induced by the insertion or extraction of lithium ions is studied in spherical particles of radius R with pre-existent internal or superficial cracks. The internal crack is disk-shaped with a diameter of $2a$, and is located in the center of the particle where the tensile stress is larger during lithiation, as shown in Figure 2a. Figure 2b shows the semi-elliptical crack, located on the particle surface where the strongest tensile stress occurs during delithiation, with semi-minor and semi-major axis a and c, respectively. The crack depth corresponds to the semi-minor axis a, instead the half width of the crack at the particle surface c' is slightly lower than the semi-axis c. However, the original semi-major axis c is considered in subsequent analyses, as c can be approximated by c' for small cracks, i.e. $R \gg a$. For sake of simplicity, the analyses are restricted to superficial circular cracks with $c = a$.

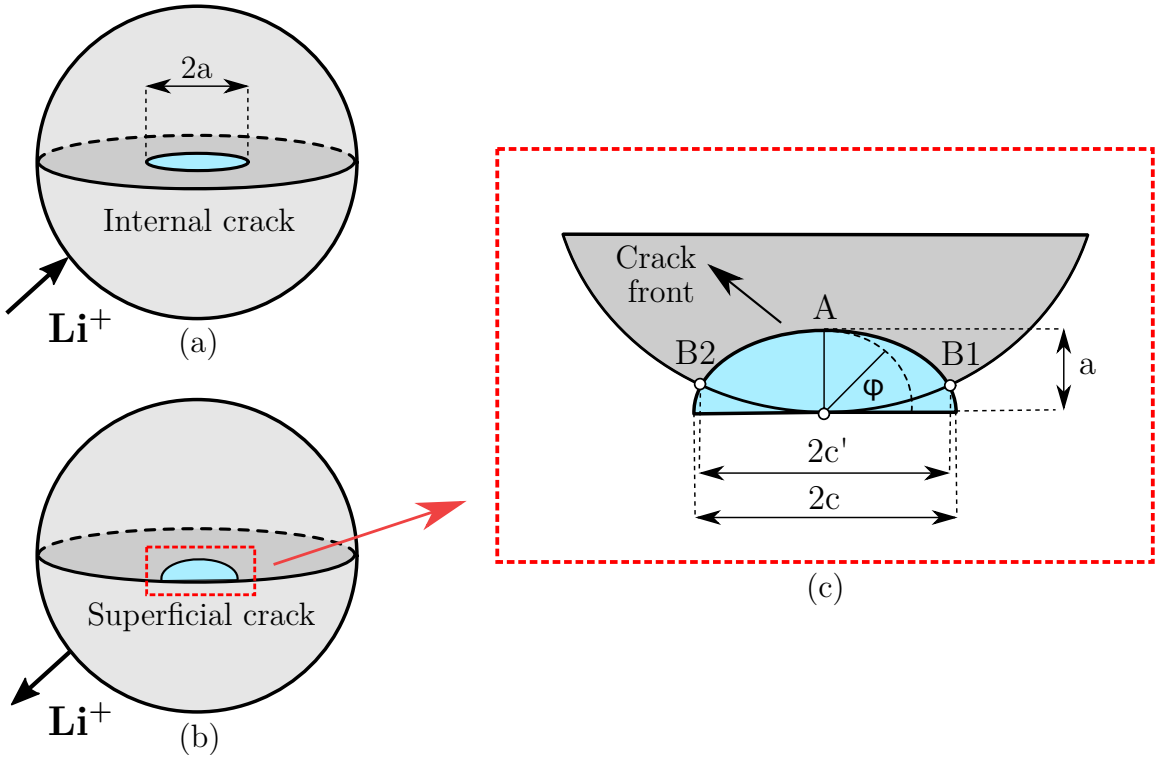

Figure 2: Sketch of a 3D spherical active material particle with pre-existent flaws: (a) disk-shaped crack located at the particle centre during lithiation, (b) semi-elliptical superficial crack during delithiation and (b) detail of the semi-elliptical superficial crack geometry in the sphere mid-plane.

The tensile hoop stress induced by the diffusion process during lithium ions insertion and extraction can drive internal cracks to grow towards the surface and surface cracks to penetrate further towards the core according to mode I, respectively. Since mode II and III toughness values, K_{IIc} and K_{IIIc}, are generally much larger than K_{Ic}, the corresponding crack face loadings can be neglected when analyzing the fracture behavior of active material particles. Based on the LEFM theory, unstable crack propagation occurs when the stress intensity factor K_I along the crack front exceeds the fracture toughness of the material K_{Ic} as shown in Equation 15. In general, K_I depends on the stress distribution over the crack area induced by the concentration gradient, which is a function of intercalation (or deintercalation) time and current density, crack geometry and the investigated position along the crack front in turn, whereas K_{Ic} is an intrinsic material parameter and can be evaluated experimentally.

3.1. FEM model

Fracture behaviour of spherical active material particles is analyzed performing a FEM-based analysis in ANSYS Mechanical APDL. The axisymmetry of the problem is exploited (Figure 3a) in order to reduce the complexity of the study in case of spherical particle with an initial central crack, whereas a 3D model is build when the initial crack is located on the particle surface (Figure 4a).

The spherical particle with central crack is modelled with 2D 8-node plane element PLANE183 in axisymmetric mode (Figure 3d). Singular elements, which are produced by collapsing one side and shifting the respective midside nodes to a quarter position (Figure 3e), are adopted in the FE model to improve the numerical results close to the crack tip [18], where the stress

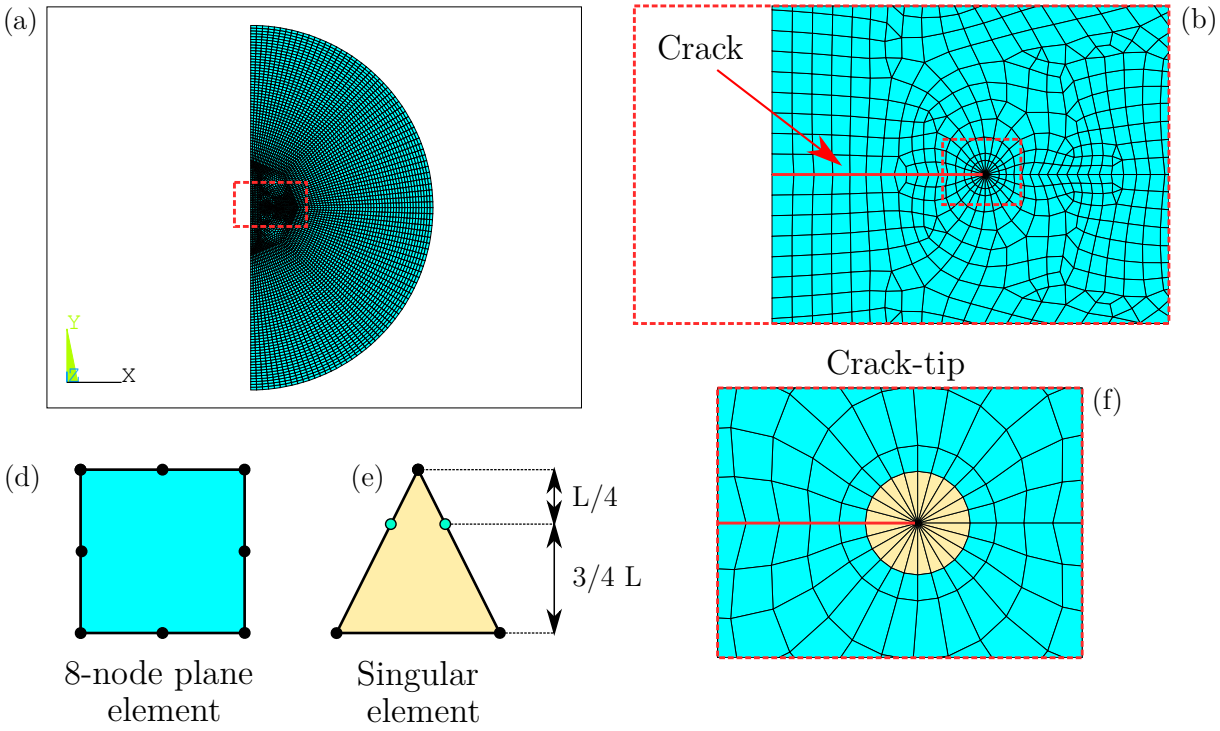

Figure 3: The 2D axisymmetric spherical particle with central crack. (a) Meshed FEM-based model with detail of (b) crack-tip region, (c) elements around crack-tip region: (d) 8-node plane element and (e) collapsed singular element with midside nodes (represented in green) at quarter-point positions.

field is singular. Since the crack tip causes a stress concentration, stress and strain gradients become larger as the crack tip is approached, therefore the elements are chosen to be small near the crack region, and their size is gradually increased when moving away from it (Figure 3b). The command of "KSCON" is used to automatically generate 12 singular elements around the specified crack-tip (Figure 3b) .

Only one half of the spherical particle in 3D model is considered, due to the symmetry of the problem. A refined mesh with collapsed quarter-point singular elements is employed in a tubular region around the crack front, to obtain a well-established singular stress field close to the crack front. Singular elements are constructed from the 15-node version of 3D isoparametric brick SOLID186 elements collapsed to wedges by shifting the mid-side nodes one-quarter away from the crack front (Figure 4e). On the top of the singular elements layer, seven additional layers, consisting of the 20-node version of isoparametric brick elements SOLID186 (Figure 4d) are added. A torus is created around the crack front to control the mesh generation. A spider web mesh made of 8 concentric rings is created on one of two meridian torus surfaces using MESH200 elements, with the innermost ring containing 12 singular elements in circumferential direction generated through the KSCON command (Figure 4g). The meshed area is then swept generating brick elements with one layer of singular elements around the crack front. A minimum of 56 elements along the crack front is used (Figure 4g). The rest of the model is meshed with 10-node tetrahedral version of SOLID186 elements (Figure 4f). Figures 4a and b show the finite element mesh of the model implementd in ANSYS. This particular mesh topology is able to accommodate different crack shapes and allows a smooth change from a refined mesh near the crack front to a larger mesh far from the crack area.

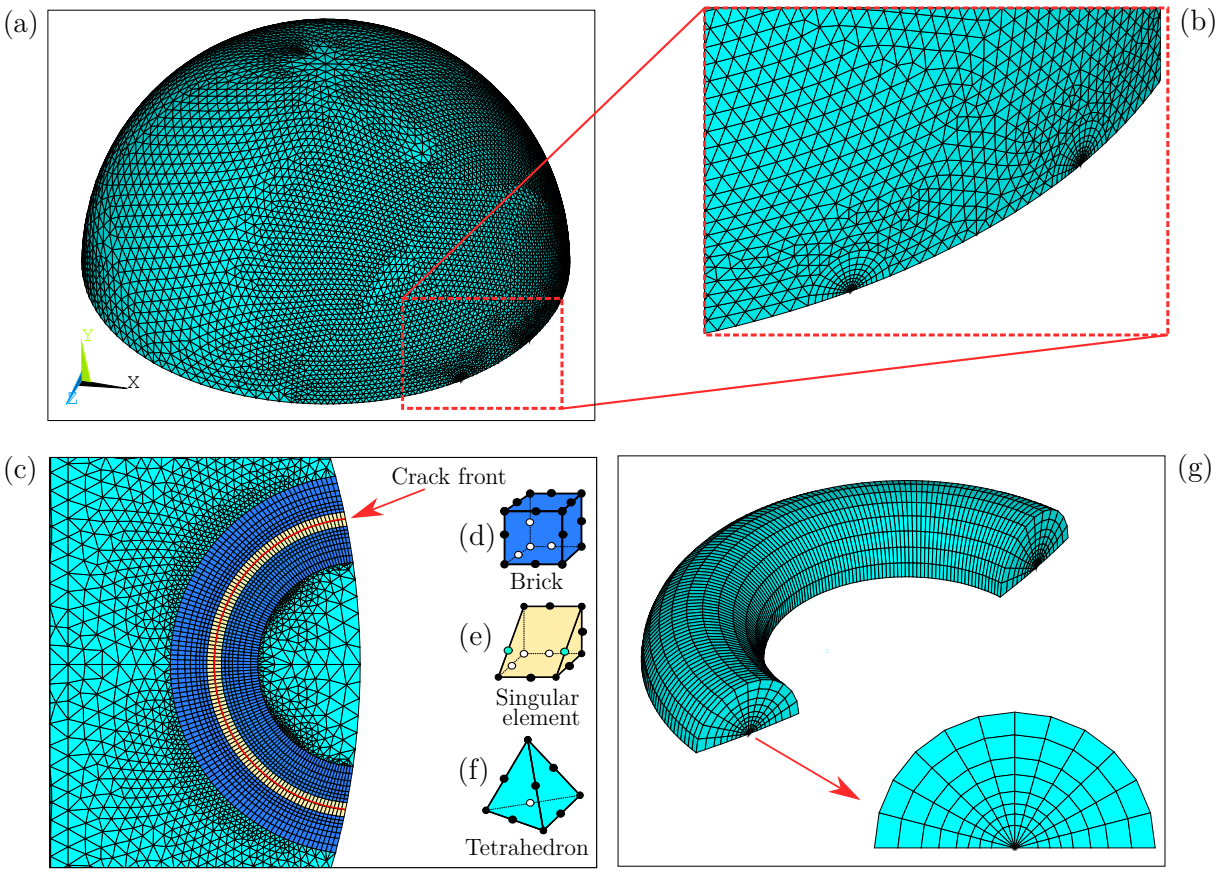

Figure 4: The 3D half spherical particle with semi-elliptical superficial crack. (a) Meshed FEM-based model with (b) detail of the crack region. (c) Bottom view of mesh around the crack region with focus on (d) 20-node brick element, (e) 15-node collapsed singular element with nodes at quarter-point positions (represented in green) and (f) 10-node tethraedral element. (g) Elements breakdown near the crack front with detail of the spider web pattern.

3.2. Simulation procedure

According to previous works [5, 6], the governing equations of lithium ions diffusion problem are similar to that of heat transfer. Exploiting the analogy between diffusive and thermal equations, the multi-physics diffusion-mechanical problem presented in section 2.1 can be reformulated with an equivalent thermal-mechanical problem by replacing the concentration distribution in the spherical particle with an equivalent temperature distribution. This allows an easier implementation in the commercial finite element software ANSYS^{TM}. In order to obtain the solution of the diffusion-mechanical problem in a faster and simpler way, the lithium concentration distribution inside the particle is computed analytically with proper mechanical and chemical boundary condition, neglecting the influence of the mechanical stress on the concentration itself [5]. The equivalent temperature gradient is shown in Equation (16) equating diffusion strain induced by the inhomogeneous chemical concentration with thermal strain.

$$\alpha(T - T_{ref}) = \frac{\Omega}{3}(C - C_{ref}) \Longrightarrow T = T_{ref} + (C - C_{ref}) \tag{16}$$

Where α is the thermal expansion coefficient, $\frac{\Omega}{3}$ is the coefficient of volume expansion due to concentration gradient, T_{ref} and C_{ref} are temperature and concentration referred to zero strain. The concentration distribution is interpolated from the centre to external surface of the particle

using a polynomial function. Based on the concentration polynomial function, the temperature field computed using Equation (16) is mapped on FE model nodes including the surface crack. The thermal induced stress and strain states, which are similar to the ones induced by the lithium diffusion inside the spherical particle, are then computed and used for the fracture mechanics analysis. A static fracture analysis is performed to evaluate the stress intensity factor K_I and to determine the subsequent crack propagation process. By assuming plane strain conditions at the tip of the central crack and at all positions along the front of the superficial crack, the K_I is computed from the J-integral value, which corresponds to the energy release rate G according to the LEFM theory:

$$K_I = \sqrt{\frac{E \cdot J}{(1-\nu^2)}} \tag{17}$$

LMO is chosen as case study to analyse the fracture in cathode intercalation materials. The LEFM theory is valid as LMO can be considered a brittle material. Lithiation and delithiation of LMO particles produce tensile hoop stresses that cause the opening of central and surperficial pre-existent crack, respectively. Lithium insertion and extraction are simulated adopting galvanostatic operation consisting of a constant lithium flux at the edge of the spherical particles. Different particle radii (R = 5, 10, 15, 20 μm), initial normalized crack depths (a/R= 0.025, 0.05, 0.1) and current densities over the particle surface (I = 1, 2, 3, 4, 5 A/m^2) are analyzed. The LMO material properties are summarized in table 2.

Table 2: LMO material properties (cathode).

Parameter	Symbol	Value	Unit	Reference
Young Modulus	E	10	GPa	[19]
Possion ratio	ν	0.3	-	[19]
Diffusion coefficient	D	$7.08 \cdot 10^{-15}$	m^2/s	[19]
Partial molar volume	Ω	$3.497 \cdot 10^{-6}$	m^3/mol	[19]
Maximum Concentration	C_{max}	$2.29 \cdot 10^4$	mol/m^3	[19]
Fracture toughness	K_{Ic}	0.24	MPa $\cdot$ m$^{1/2}$	[20]

4. Simulation results and discussion

4.1. Concentration and stress analysis

The lithium ions concentration field inside the LMO spherical particle without initial defects is computed based on the analytical model introduced in section 2.1. Exploiting the thermal analogy, diffusion induced radial and hoop stresses are then evaluated with the 2D and 3D FE models in ANSYS and compared with the analytical solution. Figure 5 shows the comparison of the results of concentration and stress state inside a particle of radius R = 10 μm during galvanostatic insertion assuming a null initial concentration within the particle and a lithium flux equivalent to a surface current density of 1 A/m^2. As previously stated, the radial stress is tensile and vanishes on the particle surface, as the interaction with surroundings is neglected and traction-free condition is assumed on the outer surface of the particle. On the contrary, the hoop stress is compressive on the surface and the largest tensile hoop stress is found to occur in the core of the particle, where pre-existing defects could lead to fracture. Figure 6 shows the comparison among FE and analytical results of concentration and stress state inside a spherical particle of radius R = 10 μm during galvanostatic extraction assuming an initial concentration

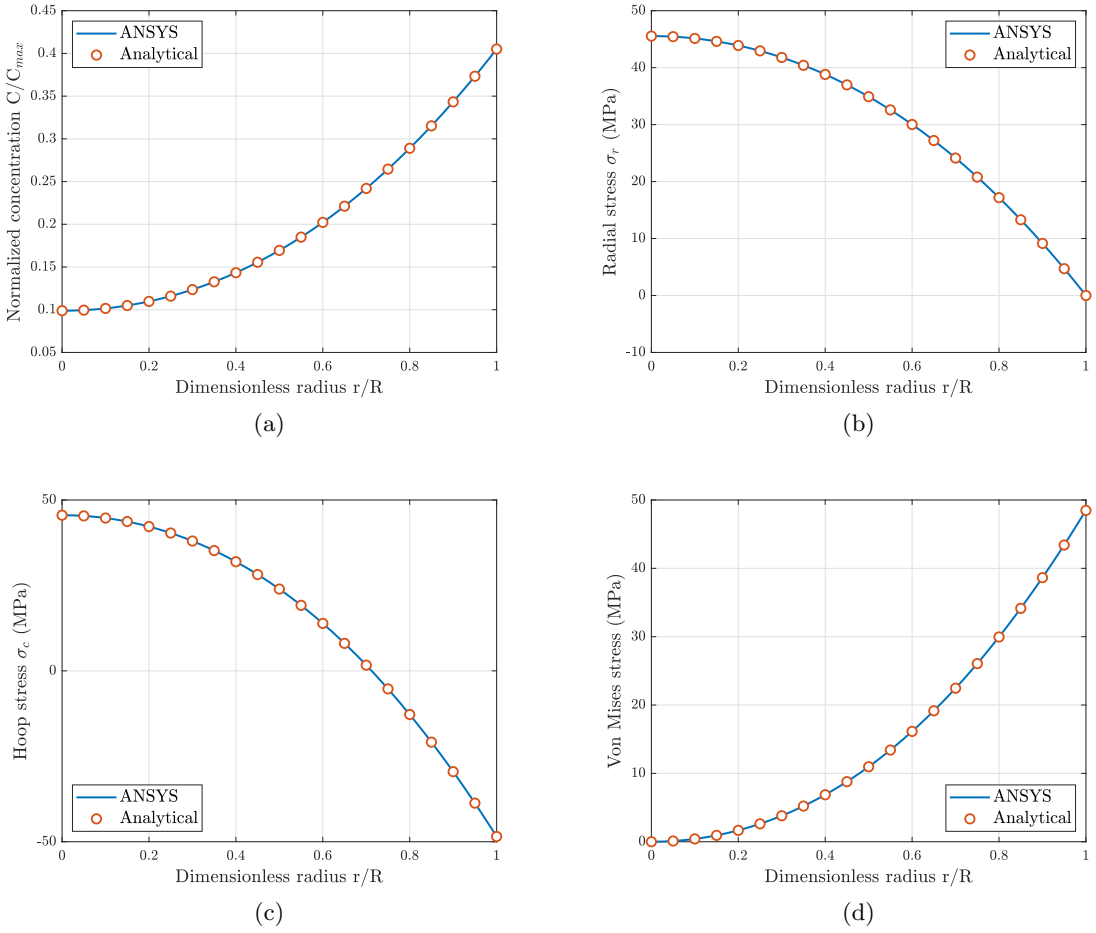

Figure 5: Comparison between analytical and FEM-based simulation results in galvanostatic insertion: (a) normalized lithium concentration C/C_{max}, (b) radial stress, (c) hoop stress and (d) Von Mises stress within a spherical particle of radius $R = 10$ μm at 1 A/m^2 current density and null initial concentration. The simulation time is equal to 2000 s.

within the particle equal to C_{max} and surface current density equal to -1 A/m^2. Radial stress is compressive and vanishes on the particle surface, on the contrary the hoop stress is compressive in the core and reaches the maximum tensile value on the particle surface, being the driving force for crack propagation.

The evolution of the hoop stress at different location along the particle radius during the lithium ions insertion and extraction processes is shown in Figure 7a and b, respectively. The hoop stress at the centre and on the surface of the particle increases monotonically at the beginning of lithiation and delithiation respectively, then it keeps constant after reaching the maximum value. Since the particle experiences the most severe loading condition at this time, it is used to compute the stress intensity factor K_I and predict if the fracture propagation occurs. Moreover, since the stress inside the particle keeps constant after an initial transient, the same stress intensity factor K_I can be computed in correspondence of almost the whole state of charge (SOC) range [5].

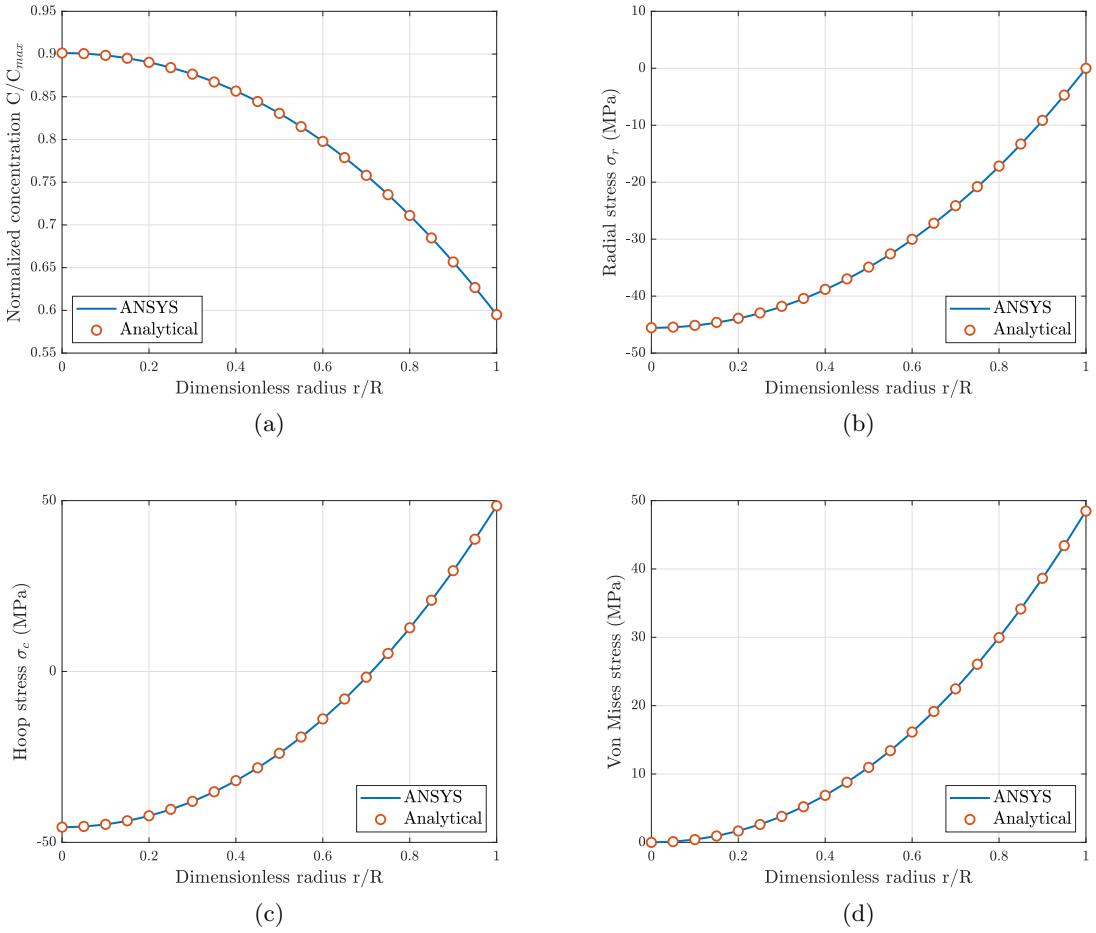

Figure 6: Comparison between analytical and FEM-based simulation results in galvanostatic extraction: (a) normalized lithium concentration C/C_{max}, (b) radial stress, (c) hoop stress and (d) Von Mises stress within a spherical particle of radius $R = 10$ μm at -1 A/m^2 current density and initial concentration $C_0 = C_{max}$. The simulation time is equal to 2000 s.

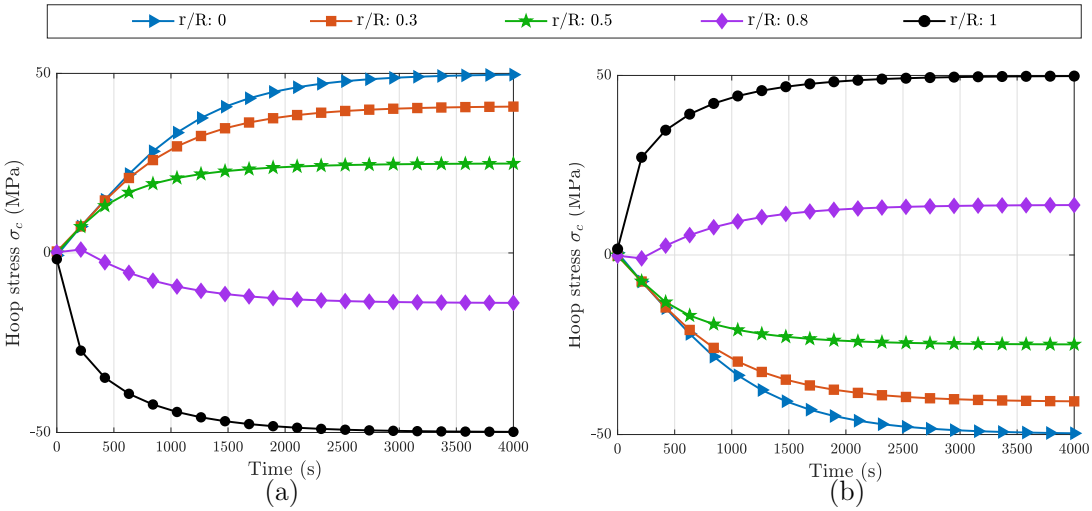

Figure 7: Hoop stress within a spherical particle of radius $R = 10$ μm as a function of diffusion time. Each curve represents a different radial position in the particle: $r/R = 0$ is the particle center and $r/R = 1$ is the particle surface. (a) galvanostatic insertion at 1 A/m^2 current density and null initial concentration and (b) galvanostatic extraction at -1 A/m^2 current density and initial concentration $C = C_{max}$.

Figure 8a shows the normalized concentration field during galvanostatic insertion, analytically computed and mapped as equivalent temperature in the 2D axisymmetric FE model of the spherical particle with central crack. Figure 8c shows the diffusion induced hoop stress distribution inside the spherical particle. Near the outer layer the particle, i.e. far from the crack region, the hoop stress distribution is compressive and relatively unaffected by the crack. On the contrary, Figure 8d shows that the particle experiences a stress singularity at the particle center close to the crack tip, according to LEFM theory.

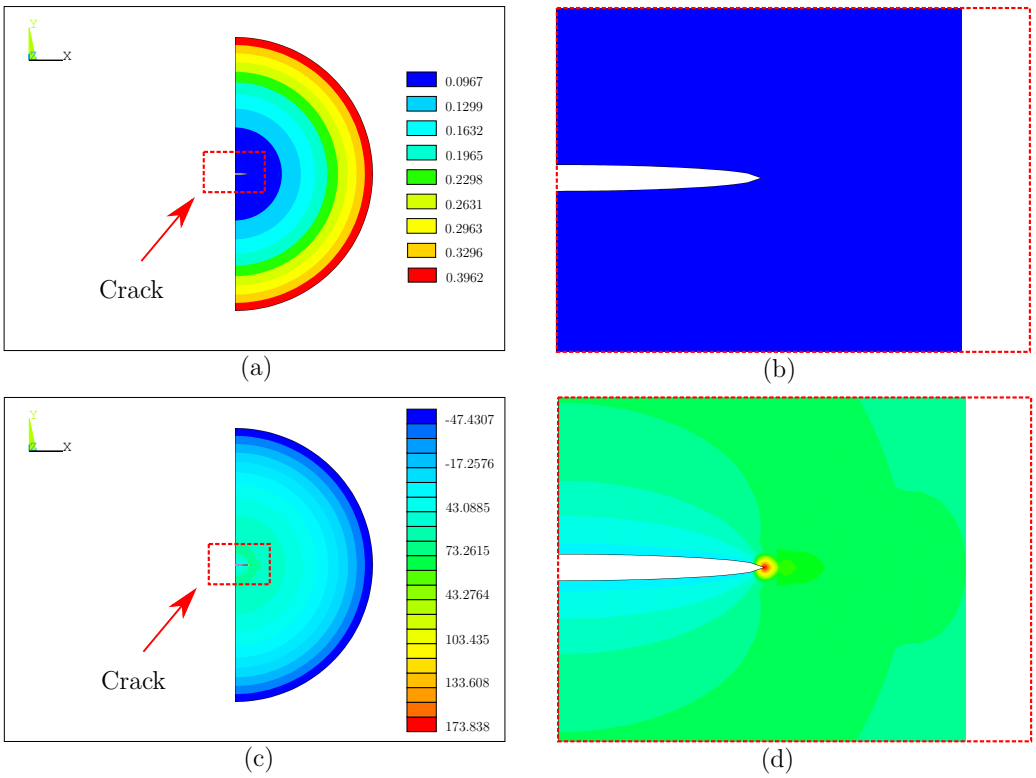

Figure 8: FE simulation results for the spherical particle of radius $R = 10$ μm, $a/R = 0.1$ during galvanostatic insertion at 1 A/m^2 current density and null initial concentration, obtained with thermal/chemical analogy. The simulation time is equal to 2000 s. (a) Normalized concentration distribution C/C_{max} with (b) detail of concentration near the crack tip region, (c) hoop stress distribution σ_c (MPa) with (d) detail of stress near the crack tip region.

Similarly, crack propagation in spherical particle with superficial pre-existing crack during lithium extraction is analysed carrying out a 3D FEM-based simulation and exploiting the thermal analogy. Lithium ions diffusion is not influenced by the crack, and the concentration distribution, shown in Figure 9a, varies from lower values in the centre of the particle to higher values on the surface resulting in higher expansion of the outer layer of the particle. Figures 9b-d show the hoop stress distribution induced by inhomogeneous volume changes inside the spherical particle. The hoop stress field away from the crack is spherically symmetric, and it is not influenced by the crack, whereas a singular stress field occurs in correspondence of the crack front.

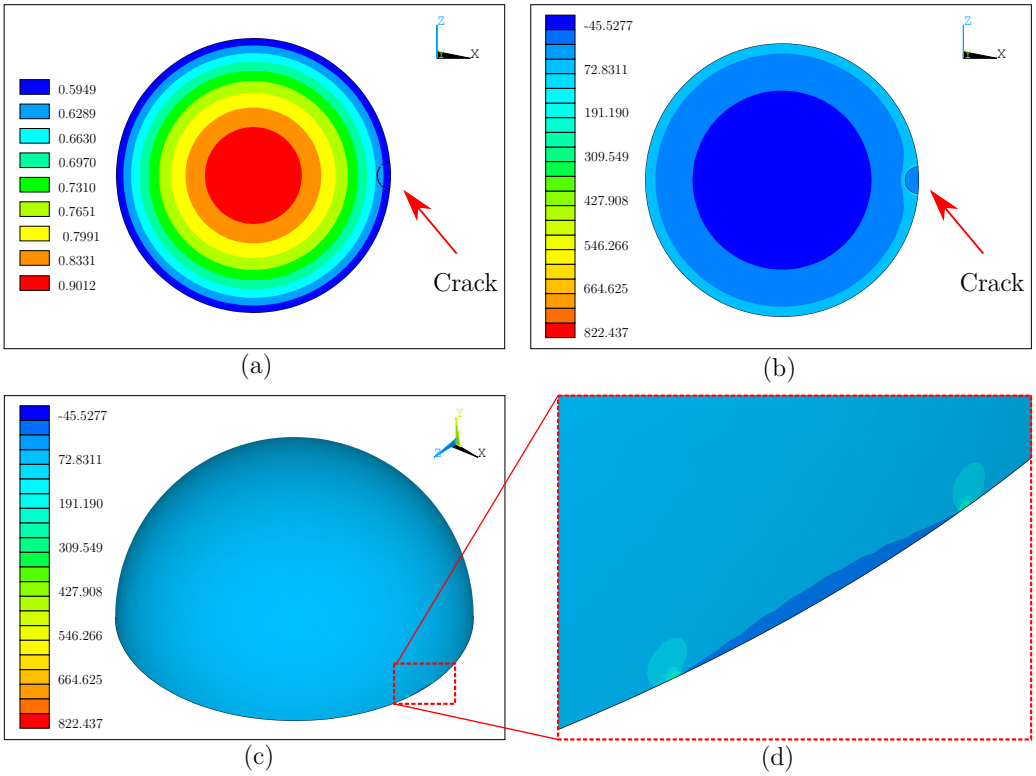

Figure 9: FE simulation results for the spherical particle of radius $R = 10$ μm, $a/R = 0.1$ during galvanostatic extraction at -1 A/m^2 current density and initial concentration equal to C_{max}, obtained with thermal/chemical analogy. The simulation time is equal to 2000 s. (a) Normalized concentration distribution C/C_{max}, hoop stress distribution σ_c (MPa) (b) inside the particle and (c) at the particle surface with (d) detail of the crack region.

4.2. Validation of the FEM model

The stress distribution in the spherical particle is used as input to compute the stress intensity factor K_I at the crack tip of central and surface cracks.

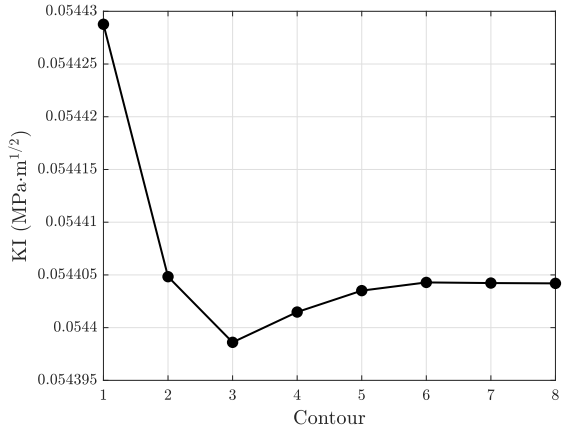

Figure 10: Stress intensity factor K_I evaluated over 8 contours in galvanostatic insertion (2000s). Particle radius $R = 10$ μm, central crack length $a/R = 0.1$ and current density $I = 1$ A/m^2.

Figure 10 shows the K_I values obtained computing the J-integral over eight different contours characterized by an increasing distance from the crack tip. The results show that K_I convergences after the fifth contour to a constant value, meaning that K_I is path-independent. The results obtained from the last contour are considered for the subsequent evaluations.

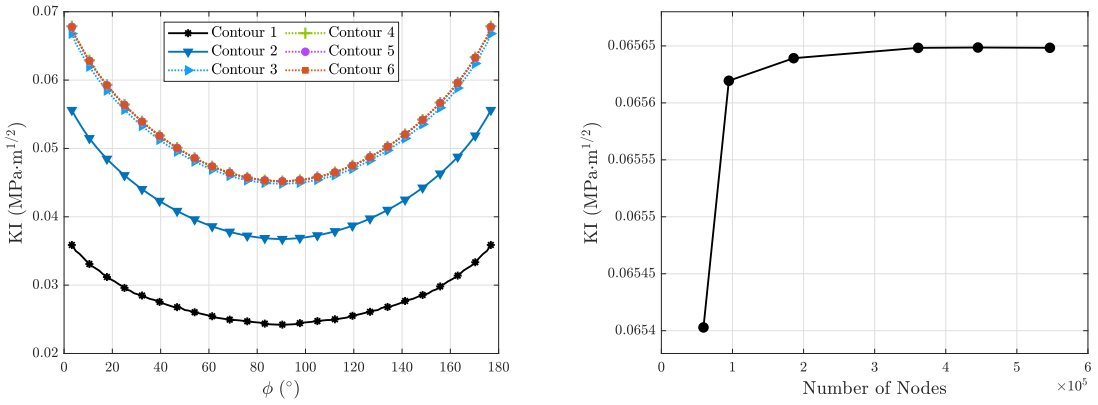

(a) (b)

Figure 11: Study of stress intensity factor K_I convergence for a spherical particle of radius $R = 10$ μm and superficial crack length $a/R = 0.1$ during galvanostatic extraction ($I = -1$ A/m^2, $t = 2000$ s): (a) K_I distribution along the crack front for six different contours. (b) K_I at point B_1 (referring to Figure 2) as a function of the number of nodes.

Figure 11a shows the stress intensity factor K_I distribution along the crack front obtained from the FEM model in galvanostatic extraction. The stress intensity factors K_I is evaluated over six contours with an increasing distance from the crack tip. The results show that K_I keeps constant when computed from the third contour, which means that the path-independence of J-integral is verified sufficiently distant from the tip. Moreover, the K_I distribution along the crack front is not uniform, but the peak value occurs at points B_1 and B_2 on the spherical surface where the hoop stress reaches its maximum value. It is highlighted that the points characterized by maximum K_I are denoted as B_1 and B_2 even if they are not directly on the spherical surface, but slightly below it. This can be explained by the existence of the so-called vertex singularity close to a corner point, i.e. where a crack front intersects the free surface in a 3D body [21], which changes the distribution of the stress field. The singularity exponent of the stress field (Equation 12) close to the free surface differs from $-1/2$. Moreover, it can be shown that the stress singularity in an elastic material must vary as $r^{-1/2}$ so that J-integral does not vanish [22]. Since K_I distribution along the crack front is computed from the J-integral, which lose their meaning on the particle surface, it is at least reasonable to assume that KI evaluated at points B_1 and B_2 have the same values as the first neighbouring crack-tip node.
In order to evaluate the 3D model reliability, a convergence test of the stress intensity factor K_I in point B_1 is performed as a function of the number of nodes. The results shown in figure 11b clearly indicate that as the number of nodes increases, the K_I converges to a constant value.

4.3. Influence of geometric factors and current density
Different simulations are performed by varying the particle radius R, normalized crack depth a/R and current density I, in order to evaluate the effect of the diffusion induced hoop stress on the particle fracture behavior and the conditions that cause the crack to propagate as well. Both central and superficial crack are analyzed. Figure 12 shows the variation of K_I as a function of particle radius R at different initial crack depths a/R.

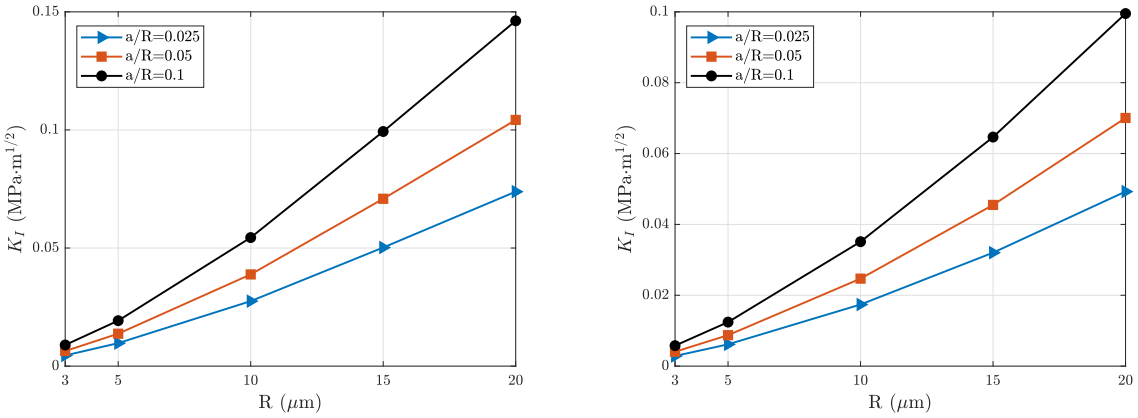

Figure 12: Stress intensity factor as a function of particle radius R and for different normalized crack depths a/R. (a) Central crack and galvanostatic insertion with current density $I = 1$ A/m^2. (b) Superficial crack and galvanostatic extraction with current density $I = -1$ A/m^2.

The stress intensity factor K_I is computed for the most severe loading condition, namely when hoop stress reaches its maximum. K_I increases monotonically with the particle radius for both galvanostatic insertion and extraction, considering a constant a/R. Smaller particles are characterized by a lower concentration gradient and consequently lower diffusion induced stress. This results in a lower K_I and greater robustness than larger particles from the fracture mechanic point of view. Moreover, for the same particle radius, the stress intensity factor K_I increases with the crack depth a/R. Indeed, a larger a/R leads the hoop stress near the crack region to increase, facilitating the fracture.
Figure 13 shows stress intensity factor computed in a particle with central crack with varying current densities I and particle radii R in galvanostatic insertion.

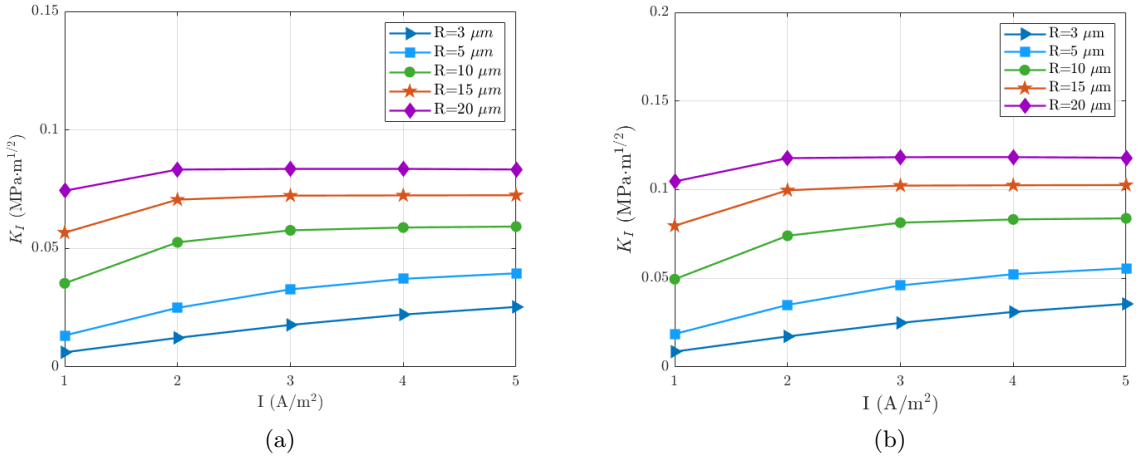

Figure 13: K_I as a function of current density I in a spherical particle with central crack during galvanostatic insertion for different particle radii R. Normalized crack depth is (a) $a/R = 0.05$ and (b) $a/R = 0.1$. Simulations are carried out for a SOC level equal to 30 %.

The current density I applied on the external surface of the particle affects the stress intensity factor as larger current densities induce higher tensile hoop stresses. As a consequence, higher

current densities are more dangerous from the crack propagation point of view, and this trend is even amplified in bigger particle. Indeed, previous works have confirmed that greater particle size results in higher stresses [5, 6], leading to higher K_I in turn. As previously highlighted, the stress intensity factor K_I always becomes greater with increasing the normalized crack depth a/R.

An increase of current density over the surface of smaller particles, namely with radius R equal to 3 and 5 μm, makes the K_I grow monotonically, whereas for particles with larger size the K_I keeps almost constant increasing the current density. This can be explained by the fact that in larger particles with higher lithium flux, i.e. current density, the concentration distribution at the particle center, where the crack is located, is fairly flat compared to the surface. Therefore, the hoop stress at the particle centre does not increases with greater current densities, as this region is barely not affected by the applied flow at the edge of the particl,e and the concentration on the surface quickly reaches the saturation value. Potentiostatic operation is needed to evaluate crack propagation during insertion properly.

Figure 14 shows the stress intensity factor K_I computed in a particle with superficial crack as a function of current density I, with different particle radii R and normalized crack depths a/R.

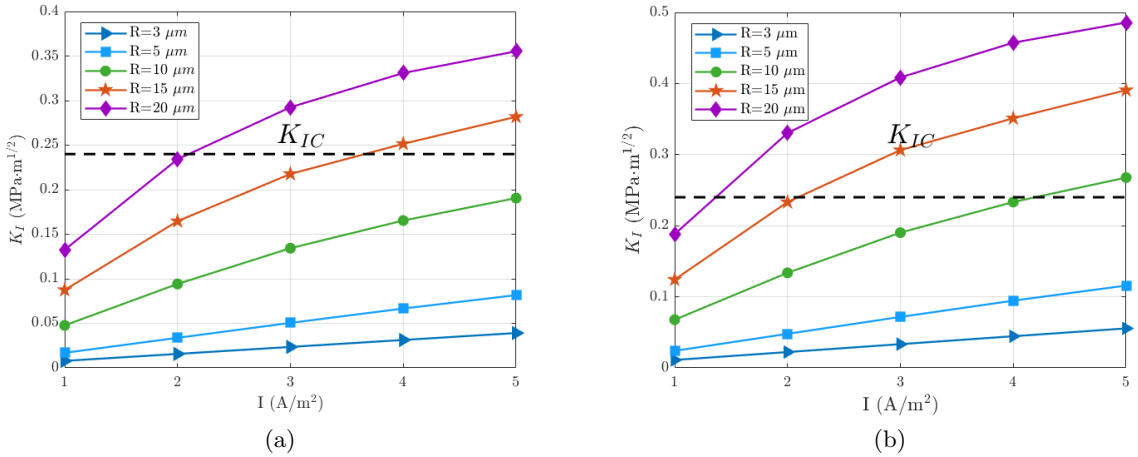

Figure 14: K_I as a function of current density I in a spherical particle with superficial crack during galvanostatic extraction for different particle radii R. Normalized crack depth is (a) $a/R = 0.05$ and (b) $a/R = 0.1$. Simulations are carried out for a SOC level equal to 30 %. The fracture toughness value K_{Ic} of LMO is reported with dashed lines.

The stress intensity factor increases with the increase the normalized crack depth a/R and the applied current density I. However, smaller particles are subjected to lower stresses, and thus lower K_I, which relieve crack propagation. Spherical particles with radius greater than 10 μm characterized by superficial crack may experience fracture, as K_I exceeds the fracture toughness K_{Ic} of LMO for certain current densities.

5. Conclusions

Fracture behaviour of active materials for lithium ion batteries is studied in this work. Mechanical stress which arises in active material due to lithium inhomogeneity are known to be the driving force of crack propagation and subsequent damage of electrode material. Starting from the electrochemical-mechanical model presented in previous works, a finite element model is built up to compute stress intensity factor in active material particles subjected to fracture. Mode I is considered, as is the one characterized by lower fracture toughness and it is the most

likely mode to cause crack propagation. Then, tensile circumferential stress is the necessary condition to have crack propagation, which occurs when stress intensity factor overcome fracture toughness of the material. Superficial and internal cracks are considered, according to the stress which is able to make the crack propagate. Indeed, during lithium insertion tensile hoop stress is present in the core of the particle, then internal cracks are likely to propagate. On the other hand, tensile hoop stress is present on the external surface during lithium deintercalation, then superficial cracks are likely to propagate. Lithium manganese oxide is chosen as case study material, considering its brittle characteristic it is suitable to LEFM hypotesis of the finite element model. Several simulations with different geometries and boundary conditions are carried out in order to evaluate when unstable propagation occurs. For what concerns geometric aspect, the results show that small particles are less likely to fracture, in agreement with the stress trend: smaller particles are characterized by lower stress as well. Then, different boundary conditions are considered, namely different current densities, proportional to the current delivered by the whole cell. Results show the combinations of particle size and current density which are safe (no unstable crack propagation) and the one that could be subjected to fracture. Potentiostatic operation will be needed to evaluate properly the propagation of central crack in bigger particles.

References

[1] Mocera F, Vergori E and Somà A 2019 Battery performance analysis for working vehicle applications *IEEE Transactions on Industry Applications* **56** 644–653
[2] Somà A, Bruzzese F, Mocera F and Viglietti E 2016 Hybridization factor and performance of hybrid electric telehandler vehicle *IEEE Transactions on Industry Applications* **52** 5130–5138
[3] Mocera F, Somà A and Clerici D 2020 Study of aging mechanisms in lithium-ion batteries for working vehicle applications *2020 Fifteenth International Conference on Ecological Vehicles and Renewable Energies (EVER)* (IEEE) pp 1–8
[4] Deshpande R, Verbrugge M, Cheng Y T, Wang J and Liu P 2012 Battery cycle life prediction with coupled chemical degradation and fatigue mechanics *Journal of the Electrochemical Society* **159** A1730
[5] Clerici D, Mocera F and Somà A 2020 Analytical solution for coupled diffusion induced stress model for lithium-ion battery *Energies* **13** 1717
[6] Clerici D and Mocera F 2021 Micro-scale modeling of lithium-ion battery *IOP Conference Series: Materials Science and Engineering* vol 1038 (IOP Publishing) p 012007
[7] Raghavan R S, Kumar A M and Narayanrao R 2015 Intercalation induced surface cracking in electrode particles *ZAMM-Journal of Applied Mathematics and Mechanics/Zeitschrift für Angewandte Mathematik und Mechanik* **95** 845–858
[8] Woodford W H, Chiang Y M and Carter W C 2010 "electrochemical shock" of intercalation electrodes: a fracture mechanics analysis *Journal of the Electrochemical Society* **157** A1052
[9] Klinsmann M, Rosato D, Kamlah M and McMeeking R M 2016 Modeling crack growth during li extraction and insertion within the second half cycle *Journal of power sources* **331** 32–42
[10] Chen B, Zhou J and Cai R 2016 Analytical model for crack propagation in spherical nano electrodes of lithium-ion batteries *Electrochimica Acta* **210** 7–14
[11] Deshpande R, Cheng Y T, Verbrugge M W and Timmons A 2011 Diffusion induced stresses and strain energy in a phase-transforming spherical electrode particle *Journal of the Electrochemical Society* **158** A718
[12] Li P, Zhao Y, Shen Y and Bo S H 2020 Fracture behavior in battery materials *Journal of Physics: Energy* **2** 022002
[13] Clerici D, Mocera F and Somà A 2021 Shape influence of active material micro-structure on diffusion and contact stress in lithium-ion batteries *Energies* **14** 134
[14] Zuo P and Zhao Y P 2015 A phase field model coupling lithium diffusion and stress evolution with crack propagation and application in lithium ion batteries *Physical Chemistry Chemical Physics* **17** 287–297
[15] Bower A F and Guduru P 2012 A simple finite element model of diffusion, finite deformation, plasticity and fracture in lithium ion insertion electrode materials *Modelling and Simulation in Materials Science and Engineering* **20** 045004
[16] Stamps M A, Eischen J W and Huang H Y S 2016 Particle-and crack-size dependency of lithium-ion battery materials lifepo 4 *AIMS Materials Science* **3** 190–203
[17] Rice J R 1968 A path independent integral and the approximate analysis of strain concentration by notches and cracks *J. Appl. Mech.* **35** 379–386

[18] Barsoum R S 1976 On the use of isoparametric finite elements in linear fracture mechanics *International journal for numerical methods in engineering* **10** 25–37
[19] Zhang X, Shyy W and Sastry A M 2007 Numerical simulation of intercalation-induced stress in li-ion battery electrode particles *Journal of the Electrochemical Society* **154** A910
[20] Mughal M Z, Amanieu H Y, Moscatelli R and Sebastiani M 2017 A comparison of microscale techniques for determining fracture toughness of limn2o4 particles *Materials* **10**
[21] Bažant Z P and Estenssoro L F 1979 Surface singularity and crack propagation *International Journal of Solids and Structures* **15** 405–426
[22] Anderson T L 2017 *Fracture Mechanics: Fumdamental and Applications* ISBN 9781498728133